HAL
open science

Fast simulation of grain growth based on Orientated Tessellation Updating Method

Daniel Weisz-Patrault, Sofia Sakout, Alain Ehrlacher

To cite this version:

Daniel Weisz-Patrault, Sofia Sakout, Alain Ehrlacher. Fast simulation of grain growth based on Orientated Tessellation Updating Method. 24 ème Congrès Français de Mécanique, Aug 2019, Brest, France. hal-02372716

HAL Id: hal-02372716

https://hal.science/hal-02372716v1

Submitted on 20 Nov 2019

HAL is a multi-disciplinary open access archive for the deposit and dissemination of scientific research documents, whether they are published or not. The documents may come from teaching and research institutions in France or abroad, or from public or private research centers.

L'archive ouverte pluridisciplinaire **HAL**, est destinée au dépôt et à la diffusion de documents scientifiques de niveau recherche, publiés ou non, émanant des établissements d'enseignement et de recherche français ou étrangers, des laboratoires publics ou privés.

Fast simulation of grain growth based on Orientated Tessellation Updating Method

D. WEISZ-PATRAULT[b,1], S. SAKOUT[a,b,2], A. EHRLACHER[a,3],

a. Navier, CNRS, École des Ponts ParisTech, 6 & 8 Ave Blaise Pascal, 77455 Marne La Vallee, France
b. LMS, École Polytechnique, CNRS, Université Paris-Saclay, 91128 Palaiseau, France
1. daniel.weisz-patrault@polytechnique.edu, 2. sofia.sakout@polytechnique.edu,
3. alain.ehrlacher@enpc.fr

Résumé :

Ce travail s'inscrit dans une idée plus générale consistant à construire un modèle macroscopique de croissance de grain dont les variables d'état contiennent en chaque point matériel, des descripteurs statistiques de la microstructure, par exemple la distribution de désorientation cristalline, la distribution de taille et forme des grains. Il s'agit de fabriquer statistiquement des potentiels d'énergie libre et de dissipation macroscopiques, sur la base d'un très grand nombre de calculs à l'échelle locale du polycristal. On en déduit in fine des lois d'évolution macroscopiques enrichies. Pour faire simple, on se place dans le cadre de la croissance de grain d'un métal monophasé sans diffusion ou ségrégation d'éléments d'alliage. Pour tester cette idée de changement d'échelle, il est donc nécessaire d'établir un outil de simulation à l'échelle du polycristal qui soit suffisamment simple et rapide pour autoriser un grand nombre de simulations sur des microstructures très variées, quitte à négliger certains détails se produisant à cette échelle. Les modélisations de croissance de grain reposant sur les éléments finis mobiles, les fonctions de niveau, les champs de phase ou la dynamique moléculaire sont trop coûteux pour être utilisées dans ce cadre. Cet article se focalise donc sur la construction d'un modèle "jouet" simple de croissance de grain. On utilise en général des outils de tessellation pour générer une approximation d'une microstructure polycristalline. On peut donc approximer l'évolution réelle de la microstructure comme une succession d'approximations par tessellation. Il devient alors assez naturel de tenter d'écrire les lois d'évolution de la microstructure directement sur les paramètres définissant la tessellation. Le modèle simplifié obtenu est très léger en terme calculatoire et permet de calculer un très grand nombre d'évolutions, dans une optique de changement d'échelle statistique.

Abstract :

This work is part of a more general idea consisting in developing a macroscopic model of grain growth whose state variables contain for each material point the statistical descriptors of the microstructure (e.g., disorientation, grain size and shape distributions). The strategy is to determine macroscopic free energy and dissipation potentials on the basis of a large number of computations at the scale of the polycrystal. The aim is to determine enriched macroscopic evolution laws. For sake of simplicity, this contribution only deals with grain growth of a single phased metal without diffusion or segregation of alloying elements. In order to test this upscaling strategy it is necessary to establish a simulation tool at the scale of the polycrystal. It should be sufficiently simple and fast to enable a large number of simulations of various microstructures, even if it leads to neglect some phenomena occurring at this scale.

Usual grain growth models relying on mobile finite element modeling, level set functions, phase field or molecular dynamics are too computationally costly to be used within the proposed framework. Therefore, this paper focuses on the development of a "toy" model. Tessellation techniques are usually used to approximate polycrystalline microstructures. Therefore, one can approximate the real evolution of the microstructure as a succession of tessellation approximations. It then becomes quite natural to attempt to establish the evolution law of the microstructure directly on the parameters defining the tessellation. The obtained model is very light in terms of computational cost and enables to compute a large number of evolutions within the framework of the proposed statistical upscaling method.

Key words : Grain Growth, Voronoi-Laguerre Tessellation, Grain Boundary Energy, Dissipation, Grain Mobility

1 Introduction

This work is part of a more general idea consisting in developing a macroscopic model of grain growth whose state variables contain for each material point the statistical descriptors of the microstructure (e.g., disorientation, grain size and shape distributions). Statistical distributions are too much detailed to be processed at each material point, thus reduced information is considered instead : means and variances at each material point. This ambition arises as very few information about microstructure is usually processed at the macroscopic scale. The general framework is the standard generalized media characterized by a free energy per unit mass and a dissipated power potential. These two potentials arise in the balance energy equation combining the first and second laws of thermodynamics. The balance energy equation should be verified for all possible virtual evolution. The two potentials depend on macroscopic state variables and their time derivatives. The determination of the macroscopic free energy and dissipation potentials enables to establish the evolution laws of the state variables characterizing the microstructure evolution at macroscale.

The strategy is to determine macroscopic free energy and dissipation potentials not axiomatically (with parametric functions) and calibration with experiments at macroscale, but on the basis of a large number of computations at the scale of the polycrystal. The aim is to quantify for each microstructure evolution the total grain boundary energy and the total dissipated power as a function of the macroscopic state variables that characterize the statistical distribution of the microstructure in order to determine enriched macroscopic evolution laws. For sake of simplicity, this contribution only deals with grain growth of a single phased metal without diffusion or segregation of alloying elements. In order to test this upscaling strategy it is necessary to establish a simulation tool at the scale of the polycrystal. It should be sufficiently simple and fast to enable a large number of simulations of various microstructures, even if it leads to neglect some phenomena occurring at this scale. Usual grain growth models relying on cellular automaton [1–4], mobile finite element modeling [5], level set functions [6, 7], phase field [8–11] or molecular dynamics [12–14] have been intensively studied and very interesting results have been obtained. However, the computational cost of such approaches is usually incompatible with an intensive use as suggested within the proposed framework. Vertex methods [15–18] consist in establishing the evolution law directly at the triple junctions and are sufficiently simple in two dimensions to reach short computation time. However, the extension in three dimensions is very difficult.

Evolution of polycrystalline microstructures (such as grain growth) involves coupled mechanisms at

different scales : (i) the atomic scale (crystal lattice), (ii) the microscale including mechanisms at grain boundaries (iii) the mesoscale revealing the grain structure (i.e., polycrystalline Representative Volume Element) and (iv) the macroscopic scale modeled as a continuous medium. Thus, this paper focuses on the development of a "toy" model formulated at mesoscale and enabling to simulate grain growth within short computation time.

Voronoi-Laguerre tessellation techniques are usually used to approximate polycrystalline microstructures at mesoscale. Very efficient algorithms have been developed with the possibility of controlling statistical distributions of grain size and shape. Crystal lattice orientation can also be specified for each grain. The tessellation equipped with such an orientation field is called an *Orientated Tessellation* (OT). One can approximate the real evolution of the microstructure as a succession of OT approximations. It then becomes quite natural to attempt to establish the evolution law of the microstructure directly on the parameters defining the OT. This modeling strategy is called in this contribution the *Orientated Tessellation Updating Method* (OTUM).

As grain growth during annealing is essentially viscous, the time derivatives of the OT parameters are obtained as a function of the thermodynamic forces defined as the partial derivatives of the total grain boundary energy with respect to the OT parameters. This mesoscale evolution law is obtained through the energy balance equation by specifying two mechanisms at microscale : (i) the grain boundary energy (disorientation) and (ii) the dissipated power by crystal visco-plasticity through any grain boundary virtual motion. For sake of simplicity, crystal lattice rotation through crystal visco-plasticity is not considered in this contribution. In addition, plane polycrystals are considered with three slip directions in each grain. Thus, the crystal lattice is plane hexagonal. This configuration corresponds to the plane $\langle 1,1,1\rangle$ of a face-centered cubic (fcc) crystal, as shown in figure 1. Disorientation between two neighboring grains (characterized by five parameters in 3D) is characterized only by two parameters in 2D : the disorientation angle $\Delta\theta$ and the orientation of the grain boundary φ. Thus, the grain boundary energy considered in this paper is computed from fcc crystals sharing the same orientation $\langle 1,1,1\rangle$ (asymmetric tilt boundaries).

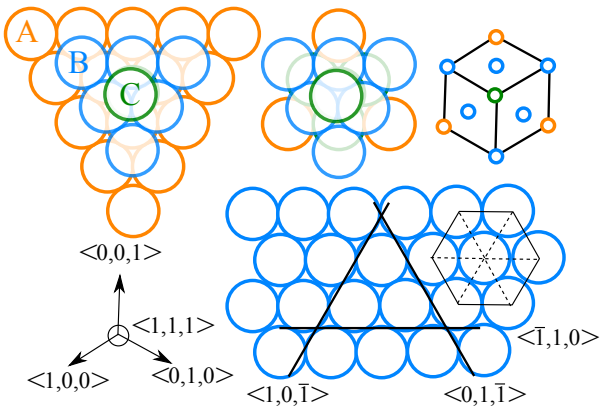

FIGURE 1 – FCC and slip directions in $\langle 1,1,1\rangle$ plane

The dissipative mechanism at microscale is calibrated to correspond to the classic notion of grain boundary mobility. The overall mesoscale grain growth model is validated by comparison with the classical curvature driven shrinkage of a spherical grain. The proposed model is very light in terms of computational cost and enables to compute a large number of microstructure evolutions, which is useful for the general statistical upscaling method.

2 Orientated Tessellation Updating Method

A tessellation is defined by n *seeds* whose Cartesian coordinates are denoted by (x_j, y_j) and n *weights* (homogeneous to the square of a radius) denoted by w_j (where $1 \leq j \leq n$). The tessellation is completely determined by the parameter vectors $\boldsymbol{x} = (x_1, \cdots, x_n)$, $\boldsymbol{y} = (y_1, \cdots, y_n)$, $\boldsymbol{w} = (w_1, \cdots, w_n)$. Each cell (or grain) denoted by C_j (where $1 \leq j \leq n$) is defined by Voronoi-Laguerre tessellation as follows :

$$C_j = \left\{ \begin{pmatrix} x \\ y \end{pmatrix} \in \mathbb{R}^2,\ \forall k \in \{1, \cdots, n\},\ \left\| \begin{matrix} x - x_j \\ y - y_j \end{matrix} \right\|^2 - w_j \leq \left\| \begin{matrix} x - x_k \\ y - y_k \end{matrix} \right\|^2 - w_k \right\} \tag{1}$$

It is clear from the definition (1) that weights are defined up to a constant. Thus, the following constrain is added to obtain a univocal definition :

$$\sum_{j=1}^{n} w_j = 1 \tag{2}$$

Thus, weights $\boldsymbol{w}$ lie in an affine hyperplane of dimension $n-1$ and denoted by $P_a^{(n-1)}$, whose support is the hyperplane denoted by $P^{(n-1)}$. In addition, it should be noted that a cell C_j may be empty as shown in figure 2. This property will be intensively used as some grains should disappear during grain growth.

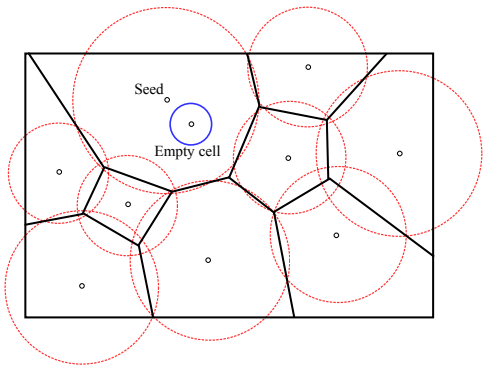

FIGURE 2 – Seed and weight in tessellation

The crystallographic orientation is denoted by $\boldsymbol{\theta} = (\theta_1, \cdots, \theta_n)$. Since the crystal lattice is plane hexagonal $\forall j \in \{1, \ldots, n\}$, $\theta_j \in \left[0, \frac{\pi}{3}\right]$. The parameter set $\mathcal{P}_{\text{OT}}$ defining the OT reads :

$$\mathcal{P}_{\text{OT}} = \left\{ \boldsymbol{\alpha} = (\boldsymbol{x}, \boldsymbol{y}, \boldsymbol{w}, \boldsymbol{\theta}) \in \mathbb{R}^n \times \mathbb{R}^n \times P_a^{(n-1)} \times \left[0, \frac{\pi}{3}\right]^n \right\} \tag{3}$$

A total energy $\mathcal{E}(T, \boldsymbol{\alpha})$ is associated to the OT, where T is the temperature. In this contribution, the total grain boundary energy per unit depth is considered. The *Orientated Tessellation Updating Method* consists in computing a time evolution of the OT characterized by $\mathcal{P}_{\text{OT}}$ by deriving an evolution law of the form :

$$\dot{\boldsymbol{\alpha}} = -\boldsymbol{M}(T, \boldsymbol{\alpha}).\frac{\partial \mathcal{E}(T, \boldsymbol{\alpha})}{\partial \boldsymbol{\alpha}} \tag{4}$$

where $\boldsymbol{M}(T, \boldsymbol{\alpha})$ is a second order tensor to be defined by introducing a dissipative mechanism at microscale and $\partial \mathcal{E}(T, \boldsymbol{\alpha}) / \partial \boldsymbol{\alpha}$ is the driving force. This paper is limited to the evolution of weights (i.e., seeds and orientations are fixed parameters : $\dot{\boldsymbol{x}} = \dot{\boldsymbol{y}} = 0$ and $\dot{\boldsymbol{\theta}} = 0$), the only state variable is $\boldsymbol{w}$.

3 Microscale mechanisms

As mentioned in the introduction, the mesoscopic evolution law (4) is determined by introducing two local mechanisms at microscale : (i) the grain boundary energy and (ii) the dissipated power by crystal visco-plasticity through any grain boundary virtual motion. Grain boundaries are indexed by pairs (i, j) where i and j denote two neighboring grains. The set of pairs of neighboring grains defining grain boundaries is denoted by I_{GB} :

$$I_{GB} = \left\{(i, j) \in \{1, \cdots, n\}^2 \,,\, j \geq i,\, C_i \cap C_j \neq \varnothing\right\} \tag{5}$$

The condition $j \geq i$ is meant to count each grain boundary only once (otherwise if $(i, j) \in I_{GB}$ then (j, i) would also be an element of I_{GB}).

The grain boundary energy per unit area of each grain $(i, j) \in I_{GB}$ is denoted E_{ij}.

$$E_{ij} = E(T, \Delta\theta_{ij}, \varphi_{ij}) \tag{6}$$

where $\Delta\theta_{ij}$ is the crystal lattice disorientation between grains i and j defined by :

$$\Delta\theta_{ij} = |\theta_j - \theta_i| \in \left[0, \frac{\pi}{3}\right] \tag{7}$$

In addition φ_{ij} is the angle of the grain boundary as shown in figure 3.

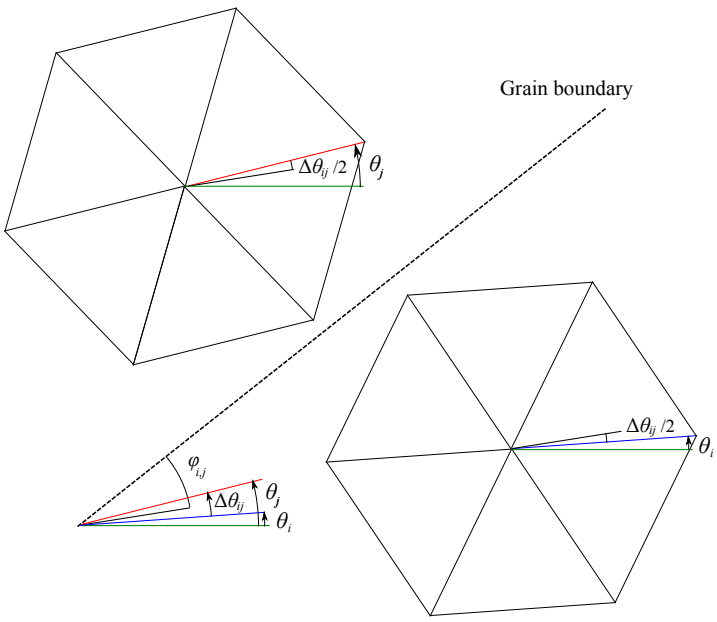

FIGURE 3 – Notations

Several analytical formulations have been proposed for E. The simplest and most widely used function is the Read & Shockley formula [19] :

$$E(T, \Delta\theta, \varphi) = E_0(T, \varphi)\Delta\theta\left[a(\varphi) - \ln(\Delta\theta)\right] \tag{8}$$

However, the range of validity of the Read & Shockley formula is limited to small disorientation angles and do not account for the energy cusps at certain disorientation angles. To overcome this difficulty,

Wolf [20] introduced a piecewise interpolation function for the grain boundary energy per unit area of the form :

$$\begin{cases} E(T,\Delta\theta,\varphi) = E_M(T,\varphi)\sin\left(\frac{\pi}{2}\frac{\Delta\theta-\Delta\theta_m}{\Delta\theta_M-\Delta\theta_m}\right)\left[1-a(\varphi)\ln\left(\sin\left(\frac{\pi}{2}\frac{\Delta\theta-\Delta\theta_m}{\Delta\theta_M-\Delta\theta_m}\right)\right)\right] \\ (\Delta\theta_m \leq \Delta\theta \leq \Delta\theta_M) \end{cases} \tag{9}$$

This interpolation function is usually fitted on atomistic simulations. Other interpolations have been proposed within a three dimensional framework [21]. Since the main goal of this contribution is to demonstrate the capability of the OTUM and not to present a study on a specific metal, a simplified grain boundary function is directly defined in the form of (9). Since the crystal lattice is plane hexagonal, a cusp is introduced at $\pi/3$. In addition it is assumed that the dependance on φ is negligible. The grain boundary energy per unit area is defined as follows :

$$E(T,\Delta\theta) = \frac{G(T)}{G(0)}\gamma(\Delta\theta) \tag{10}$$

where $G(T)$ is the shear coefficient. In this paper, data for pure iron [22] are used to calibrate $G(T)$:

$$G(T) = a_G\,T + b_G \tag{11}$$

where $b_G \approx 88134$ MPa and $a_G \approx -24$ MPa.K^{-1}. The temperature dependence $G(T)/G(0)$ is a simple choice similar to [23]. In addition :

$$\begin{cases} \gamma(\Delta\theta) = \gamma_{\frac{\pi}{6}}\sin(3\Delta\theta)\left[1-a_1\ln(\sin(3\Delta\theta))\right] \\ \left(0 \leq \Delta\theta \leq \frac{\pi}{6}\right) \\ \gamma(\Delta\theta) = \gamma_{\frac{\pi}{6}}\sin(\pi-3\Delta\theta)\left[1-a_2\ln(\sin(\pi-3\Delta\theta))\right] \\ \left(\frac{\pi}{6} \leq \Delta\theta \leq \frac{\pi}{3}\right) \end{cases} \tag{12}$$

where $a_1 = a_2 = 1$ and $\gamma_{\frac{\pi}{6}} = 1$ J.m^{-2}, which roughly corresponds to pure iron. The resulting simplified grain boundary energy per unit area is presented in figure 4.

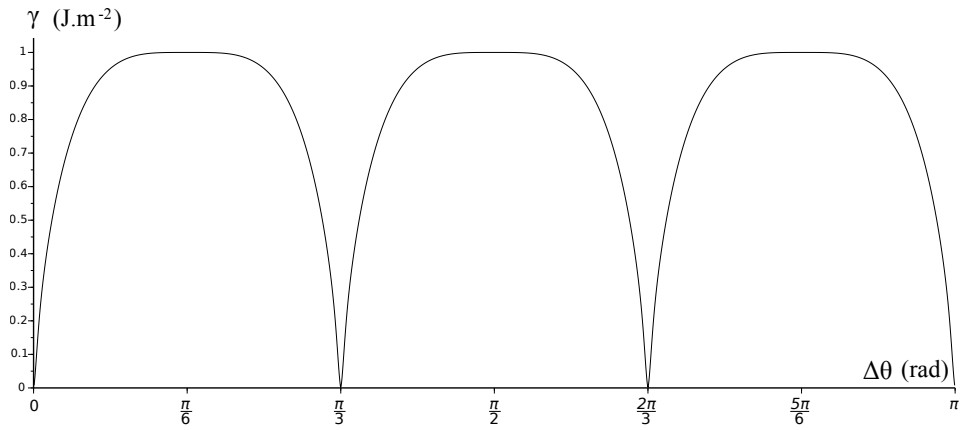

FIGURE 4 – Grain boundary energy per unit area at $T = 0$ K

In addition to the grain boundary energy per unit area, the dissipated power per unit area through any

virtual grain boundary motion should be specified. Consider v_{ij}^* a virtual normal velocity of the grain boundary $(i,j) \in I_{GB}$. The dissipated power per unit area reads :

$$D_{ij}^* = D(T, \Delta\theta_{ij}, v_{ij}^*) \tag{13}$$

where [24, 25] used crystal plasticity to determine D analytically (for plane hexagonal crystals) when the boundary between two semi-infinite crystals moves at the virtual velocity v_{ij}^* :

$$D(T, \Delta\theta_{ij}, v_{ij}^*) = \tau_c X(\Delta\theta_{ij}) \left|v_{ij}^*\right| \tag{14}$$

where τ_c is the critical shear stress and $X : \Delta\theta \mapsto X(\Delta\theta)$ is the following function :

$$X(\Delta\theta) = \frac{6}{\pi}\left(\frac{\pi}{3} + 2\sqrt{3}\ln\left(\frac{\sqrt{3}}{2}\right)\right)\min\left\{\Delta\theta, \frac{\pi}{3} - \Delta\theta\right\} \tag{15}$$

Since grain growth is viscous, the analytical computation proposed by [24, 25] is simply adapted for crystal visco-plasticity by considering that the critical shear stress τ_c linearly depends on $\left|v_{ij}^*\right|$:

$$\tau_c = \frac{\left|v_{ij}^*\right|}{m(T)} \tag{16}$$

where the function $m(T)$ is homogenous to a grain mobility (m^4.J^{-1}.s^{-1}). Hence the dissipated power per unit area :

$$D(T, \Delta\theta_{ij}, v_{ij}^*) = \frac{X(\Delta\theta_{ij})}{m(T)}\left[v_{ij}^*\right]^2 \tag{17}$$

It should be noted from (9) and (15) that :

$$\begin{cases} \gamma(\Delta\theta) \underset{\Delta\theta\to 0}{\sim} A\Delta\theta\ln(\Delta\theta) \\ X(\Delta\theta) \underset{\Delta\theta\to 0}{\sim} B\Delta\theta \end{cases} \tag{18}$$

In other words, the driving force (proportional to $\gamma(\Delta\theta)$) tends to zero when the disorientation tends to zero. However, the dissipative cost (proportional to $X(\Delta\theta)$) that resists to the driving force, tends to zero much faster because of the logarithmic term in (18). Thus, for arbitrarily small disorientation, the grain boundary is unstable as the driving force is arbitrarily large in comparison to the resistive mechanism (the ratio is in $\ln(\Delta\theta)$).

4 Mesoscale evolution law

The mesoscale evolution law is derived by considering the total grain boundary energy per unit depth and the total dissipated power per unit depth through any virtual grain boundary normal velocity field, which are defined as follows :

$$\begin{cases} \mathcal{E}(T, \boldsymbol{\alpha}) = \sum\limits_{(i,j)\in I_{GB}} l_{ij}E_{ij} \\ \mathcal{D}(T, \boldsymbol{\alpha}, \boldsymbol{v}^*) = \sum\limits_{(i,j)\in I_{GB}} l_{ij}D_{ij}^* \end{cases} \tag{19}$$

where l_{ij} the joint length and $\boldsymbol{v}^* = \left(v^*_{ij}\right)_{(i,j)\in I_{GB}}$. The dependance on $\boldsymbol{\alpha} = (\boldsymbol{x}, \boldsymbol{y}, \boldsymbol{w}, \boldsymbol{\theta})$ comes from the grain boundary lengths l_{ij} that depend on $(\boldsymbol{x}, \boldsymbol{y}, \boldsymbol{w})$ and E_{ij}, D^*_{ij} that depend on $\boldsymbol{\theta}$. The number of grain boundary is $n_{GB} = \text{card}\,[I_{GB}]$. There exists a bijection between I_{GB} and $\{1, \cdots, n_{GB}\}$ that defines the numbering of grain boundaries. Thus, for each grain boundary denoted by $(i, j) \in I_{GB}$ there exists a unique $p_{ij} \in \{1, \cdots, n_{GB}\}$. Therefore the total dissipated power per unit area reads :

$$\mathcal{D}(T, \boldsymbol{\alpha}, \boldsymbol{v}^*) = \boldsymbol{v}^*.\frac{\boldsymbol{\chi}(\boldsymbol{\alpha})}{m(T)}.\boldsymbol{v}^* \tag{20}$$

where $\boldsymbol{\chi}(\boldsymbol{\alpha})$ is a diagonal second order tensor of size $n_{GB} \times n_{GB}$ of diagonal :

$$\forall p_{ij} \in \{1, \cdots, n_{GB}\}\,,\ \chi_{p_{ij}}(\boldsymbol{\alpha}) = l_{ij} X(\Delta\theta_{ij}) \tag{21}$$

As seeds and crystalline orientations are fixed (i.e., $\dot{\boldsymbol{x}} = \dot{\boldsymbol{y}} = 0$ and $\dot{\boldsymbol{\theta}} = 0$) and considering any virtual variation of weights $\dot{\boldsymbol{w}}^*$, it is straightforward to demonstrate that :

$$v^*_{ij} = \frac{\dot{w}^*_i - \dot{w}^*_j}{2d_{ij}} \tag{22}$$

where d_{ij} is the distance between seeds :

$$d_{ij} = \left\| \begin{pmatrix} x_i \\ y_i \end{pmatrix} - \begin{pmatrix} x_j \\ y_j \end{pmatrix} \right\| \tag{23}$$

It is clear in (22) that for each grain boundary an arbitrary choice is made for the positive direction of the normal velocity v^*_{ij}, which has no consequence as the square of the virtual velocity arises in the dissipated power. Hence :

$$\boldsymbol{v}^* = \boldsymbol{K}(\boldsymbol{\alpha}).\dot{\boldsymbol{w}}^* \tag{24}$$

where $\boldsymbol{K}(\boldsymbol{\alpha})$ is a second order tensor of size $n_{GB} \times n$, which can be evaluated analytically :

$$\boldsymbol{K}(\boldsymbol{\alpha}) = \begin{array}{c} \\ p_{ij} \end{array} \begin{array}{c} \begin{array}{ccccccccccc} & & & i & & & & j & & & \end{array} \\ \begin{pmatrix} \vdots & \vdots & \vdots & \vdots & \vdots & \vdots & \vdots & \vdots & \vdots & \vdots & \vdots \\ 0 & \cdots & 0 & \frac{1}{2d_{ij}} & 0 & \cdots & 0 & -\frac{1}{2d_{ij}} & 0 & \cdots & 0 \\ \vdots & \vdots & \vdots & \vdots & \vdots & \vdots & \vdots & \vdots & \vdots & \vdots & \vdots \end{pmatrix} \end{array} \tag{25}$$

The constrain (2) leads to :

$$\sum_{j=1}^{n} \dot{w}^*_j = 0 \tag{26}$$

which defines a hyperplane of dimension $n-1$ denoted by $P^{(n-1)}$, whose normal vector is denoted by $\mathbf{1} = (1, \cdots, 1) \in \mathbb{R}^n$. It is clear that the kernel of $\boldsymbol{K}(\boldsymbol{\alpha})$ is $\ker(\boldsymbol{K}(\boldsymbol{\alpha})) = \mathbf{1}\,\mathbb{R}$. The total dissipated power per unit depth reads :

$$\mathcal{D}(T, \boldsymbol{\alpha}, \boldsymbol{v}^*) = \dot{\boldsymbol{w}}^*.\frac{\boldsymbol{R}(\boldsymbol{\alpha})}{m(T)}.\dot{\boldsymbol{w}}^* \tag{27}$$

where $\boldsymbol{R}(\boldsymbol{\alpha}) = \boldsymbol{K}(\boldsymbol{\alpha})^T.\boldsymbol{\chi}(\boldsymbol{\alpha}).\boldsymbol{K}(\boldsymbol{\alpha})$ is a second order tensor of size $n \times n$.

The "real" weight variation $\dot{\boldsymbol{w}}$ (considered as the solution among all possible virtual weight variations

$\dot{\boldsymbol{w}}^*$) is determined for isothermal (i.e., $\dot{T} = 0$) and homogenous temperature fields (i.e., $\boldsymbol{\nabla} T = 0$) by using the general energy balance equation (combining the first and second thermodynamic laws), which reads :

$$\dot{\mathcal{E}} + \mathcal{D} = 0 \tag{28}$$

Hence :

$$[\dot{\boldsymbol{w}}] \, . \left(\frac{\partial \mathcal{E}}{\partial \boldsymbol{w}} + \frac{\boldsymbol{R}(\boldsymbol{\alpha})}{m(T)} . \dot{\boldsymbol{w}} \right) = 0 \tag{29}$$

Using the maximum dissipation principle, the evolution law reads :

$$\boldsymbol{R}(\boldsymbol{\alpha}) . \dot{\boldsymbol{w}} = -m(T) \frac{\partial \mathcal{E}(T, \boldsymbol{\alpha})}{\partial \boldsymbol{w}} \tag{30}$$

The evolution law (30) should be inverted. However $\boldsymbol{R}(\boldsymbol{\alpha})$ is not invertible because of the constrain (26). The kernel of $\boldsymbol{R}(\boldsymbol{\alpha})$ is $\ker(\boldsymbol{R}(\boldsymbol{\alpha})) = \mathbf{1}\,\mathbb{R}$. Thus, there are $n-1$ strictly positive singular values of $\boldsymbol{R}(\boldsymbol{\alpha})$ denoted by $(\lambda_1, \cdots, \lambda_{n-1})$ and there exist two orthogonal tensors $\boldsymbol{U}$ and $\boldsymbol{V}$ such as :

$$\boldsymbol{R}(\boldsymbol{\alpha}) = \boldsymbol{U} . \left(\begin{array}{ccc|c} \lambda_1 & \cdots & 0 & \\ \vdots & \ddots & \vdots & 0 \\ 0 & \cdots & \lambda_{n-1} & \\ \hline & 0 & & 0 \end{array} \right) . \boldsymbol{V} \tag{31}$$

The singular value decomposition is computed in *Scilab* [26] and gives $(\lambda_1, \cdots, \lambda_{n-1})$, $\boldsymbol{U}$ and $\boldsymbol{V}$. The *Moore-Penrose* pseudo-inverse matrix is introduced as follows :

$$\boldsymbol{\Sigma}^\dagger = \left(\begin{array}{ccc|c} \frac{1}{\lambda_1} & \cdots & 0 & \\ \vdots & \ddots & \vdots & 0 \\ 0 & \cdots & \frac{1}{\lambda_{n-1}} & \\ \hline & 0 & & 0 \end{array} \right) \tag{32}$$

Hence the evolution law :

$$\dot{\boldsymbol{w}} = -m(T) \boldsymbol{M}(\boldsymbol{\alpha}) . \frac{\partial \mathcal{E}(T, \boldsymbol{\alpha})}{\partial \boldsymbol{w}} \tag{33}$$

where :

$$\boldsymbol{M}(\boldsymbol{\alpha}) = \left(\boldsymbol{V}^T . \boldsymbol{\Sigma}^\dagger . \boldsymbol{U}^T \right) \tag{34}$$

5 Driving force

The driving force involved in the evolution law (33) should be evaluated. An analytic solution is derived in this section, which contributes to reach short computation time. From (19) and (10) one obtains :

$$\mathcal{E}(T, \boldsymbol{\alpha}) = \frac{G(T)}{G(0)} \sum_{(i,j) \in I_{GB}} l_{ij} \gamma(\Delta\theta_{ij}) \tag{35}$$

Hence :

$$\frac{\partial \mathcal{E}(T, \boldsymbol{\alpha})}{\partial \boldsymbol{w}} = \frac{G(T)}{G(0)} \sum_{(i,j) \in I_{GB}} \frac{\partial l_{ij}}{\partial \boldsymbol{w}} \gamma(\Delta\theta_{ij}) \tag{36}$$

Consider the set of triple junctions :

$$I_3 = \left\{ (i,j,k) \in \{1,\cdots,n\}^3 \,,\, C_i \cap C_j \cap C_k \neq \varnothing \right\} \tag{37}$$

There is no condition such as $k \geq j \geq i$, thus if $(i,j,k) \in I_3$ then all permutations are also in I_3. Consider the third order tensor $\boldsymbol{\delta}$:

$$\widetilde{\delta}_{ijk} = \begin{cases} 1 & \text{if} \quad (i,j,k) \in I_3 \\ 0 & \text{if} \quad (i,j,k) \notin I_3 \end{cases} \tag{38}$$

Thus, the third order tensor $\boldsymbol{\beta}$ representing angles at the triple junctions as shown in figure 5 are defined as follows :

$$\beta_{ijk} = \begin{cases} \beta_{ijk} & \text{if} \quad (i,j,k) \in I_3 \\ \dfrac{\pi}{2} & \text{if} \quad (i,j,k) \notin I_3 \end{cases} \tag{39}$$

where the following symmetry rule holds $\beta_{ijk} = \beta_{kji}$.

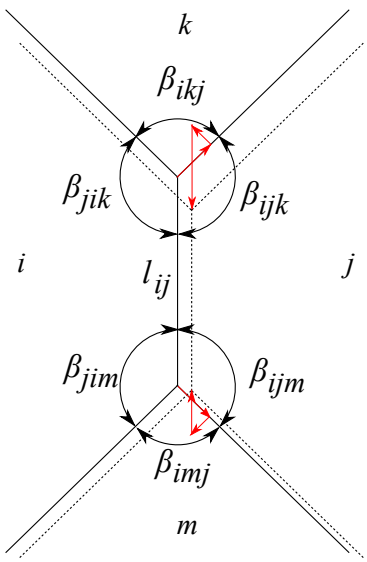

FIGURE 5 – Triple junctions

Consider a virtual weight variation $\dot{\boldsymbol{w}}^* \in P^{(n-1)}$ (i.e., verifying the constrain (26)). One obtains :

$$\begin{aligned} \dot{l}_{ij} = \; & \frac{\tan\left(\beta_{ijk} - \frac{\pi}{2}\right) + \tan\left(\beta_{ijm} - \frac{\pi}{2}\right)}{2d_{ij}} \dot{w}_i^* + \frac{\tan\left(\beta_{jik} - \frac{\pi}{2}\right) + \tan\left(\beta_{jim} - \frac{\pi}{2}\right)}{2d_{ij}} \dot{w}_j^* \\ & - \frac{1}{2d_{jk}\cos\left(\beta_{ijk} - \frac{\pi}{2}\right)} \dot{w}_k^* - \frac{1}{2d_{jm}\cos\left(\beta_{ijm} - \frac{\pi}{2}\right)} \dot{w}_m^* \end{aligned} \tag{40}$$

Moreover :

$$\dot{l}_{ij} = \left(\frac{\partial l_{ij}}{\partial \boldsymbol{w}} \right) . \dot{\boldsymbol{w}}^* \tag{41}$$

Hence by combining (40) and (41) and $\partial l_{ij}/\partial \boldsymbol{w} = \left(\partial l_{ij}/\partial w_q\right)_{q \in \{1,\cdots,n\}}$:

$$\frac{\partial l_{ij}}{\partial w_q} = \sum_{p=1}^{n} \widetilde{\delta}_{ijp} \left(\frac{\tan\left(\beta_{ijp} - \frac{\pi}{2}\right)}{2d_{ij}} \delta_{iq} + \frac{\tan\left(\beta_{jip} - \frac{\pi}{2}\right)}{2d_{ij}} \delta_{jq} - \frac{\delta_{pq}}{2d_{jp}\cos\left(\beta_{ijp} - \frac{\pi}{2}\right)} \right) \tag{42}$$

where δ is the Kronecker symbol.

6 Calibration

The proposed approach is calibrated by comparison with the classic curvature driven grain growth. Within this framework, the driving force acting on any grain boundary reads :

$$\widetilde{F} = \frac{G(T)}{G(0)}\gamma(\Delta\theta)\left(\frac{1}{R^I} + \frac{1}{R^{II}}\right) \tag{43}$$

Where R^I and R^{II} are the radii of curvature along the principal directions (in three dimensions). For plane polycrystals $R_I = R$ and $R_{II} = \infty$. A simple linear evolution law accounting for viscosity is usually used :

$$\widetilde{v} = \widetilde{m}(T, \Delta\theta)\,\widetilde{F} \tag{44}$$

Where $\widetilde{v}$ is the inward normal speed of the considered grain boundary and $\widetilde{m}(T, \Delta\theta)$ the classical grain boundary mobility for the curvature driven model (where the symbol $\widetilde{.}$ refers to the *curvature driven* model). In the following, a circular grain shrinkage is compared to an hexagonal configuration as shown in figure 6 in order to determine the mobility $m(T)$ introduced in the dissipated power (16) as a function of $\widetilde{m}(T, \Delta\theta)$. Thus for the curvature driven model the inward normal speed reads :

$$\widetilde{v} = \widetilde{m}(T, \Delta\theta)\frac{G(T)}{G(0)}\frac{\gamma(\Delta\theta)}{R} \tag{45}$$

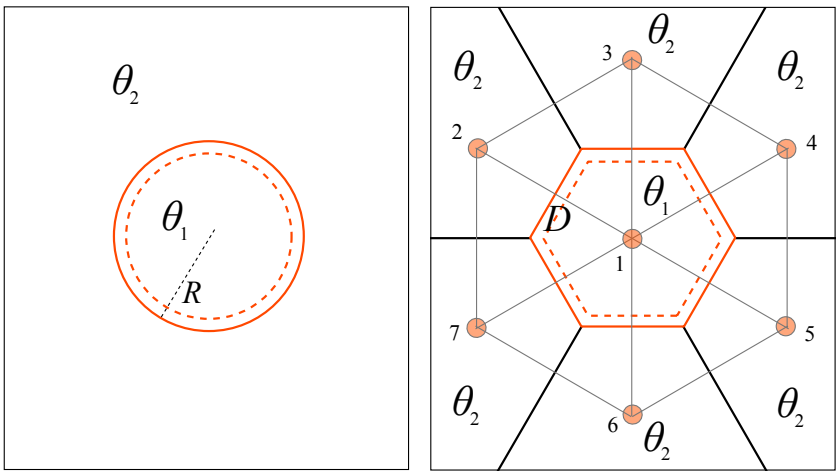

FIGURE 6 – Validation by comparison to curvature driven spherical grain shrinkage

The proposed approach is applied to the hexagonal situation. The partial derivative (42) reads :

$$\begin{aligned} &\forall j \in \{2, \cdots, 7\} \\ &\frac{\partial l_{1j}}{\partial w_1} = \frac{\partial l_{1j}}{\partial w_j} = -\frac{\partial l_{1j}}{\partial w_{j-1}} = -\frac{\partial l_{1j}}{\partial w_{j+1}} = \frac{1}{2\sqrt{3}R} \end{aligned} \tag{46}$$

Hence :

$$\begin{aligned}
\frac{\partial l_{12}}{\partial \boldsymbol{w}} &= \frac{1}{2\sqrt{3}R}\,(1,1,-1,0,0,0,-1)^T & \frac{\partial l_{13}}{\partial \boldsymbol{w}} &= \frac{1}{2\sqrt{3}R}\,(1,-1,1,-1,0,0,0)^T \\
\frac{\partial l_{14}}{\partial \boldsymbol{w}} &= \frac{1}{2\sqrt{3}R}\,(1,0,-1,1,-1,0,0)^T & \frac{\partial l_{15}}{\partial \boldsymbol{w}} &= \frac{1}{2\sqrt{3}R}\,(1,0,0,-1,1,-1,0)^T \\
\frac{\partial l_{16}}{\partial \boldsymbol{w}} &= \frac{1}{2\sqrt{3}R}\,(1,0,0,0,-1,1,-1)^T & \frac{\partial l_{17}}{\partial \boldsymbol{w}} &= \frac{1}{2\sqrt{3}R}\,(1,-1,0,0,0,-1,1)^T
\end{aligned} \tag{47}$$

The driving force (36) reads :

$$\frac{\partial \mathcal{E}(T,\boldsymbol{\alpha})}{\partial \boldsymbol{w}} = \frac{G(T)}{G(0)}\frac{\gamma(\Delta\theta)}{2\sqrt{3}R}\,(6,-1,-1,-1,-1,-1,-1)^T \tag{48}$$

The second order tensor $\boldsymbol{K}$ introduced in (25) reads for this configuration :

$$\boldsymbol{K} = \begin{array}{c} \\ p_{12} \\ p_{13} \\ p_{14} \\ p_{15} \\ p_{16} \\ p_{17} \end{array} \begin{array}{c} \begin{array}{ccccccc} 1 & 2 & 3 & 4 & 5 & 6 & 7 \end{array} \\ \begin{pmatrix} -1 & 1 & 0 & 0 & 0 & 0 & 0 \\ -1 & 0 & 1 & 0 & 0 & 0 & 0 \\ -1 & 0 & 0 & 1 & 0 & 0 & 0 \\ -1 & 0 & 0 & 0 & 1 & 0 & 0 \\ -1 & 0 & 0 & 0 & 0 & 1 & 0 \\ -1 & 0 & 0 & 0 & 0 & 0 & 1 \end{pmatrix} \end{array} \frac{1}{4R} \tag{49}$$

The second order tensor $\boldsymbol{\chi}$ introduced in (21) reads :

$$\boldsymbol{\chi} = \frac{R}{\sqrt{3}} X(\Delta\theta)\boldsymbol{I} \tag{50}$$

where $\boldsymbol{I}$ is the identity of size 6×6. The second order tensor $\boldsymbol{R}$ introduced in (27) reads :

$$\boldsymbol{R} = \boldsymbol{K}^T.\boldsymbol{\chi}.\boldsymbol{K} = \frac{X(\Delta\theta)}{16\sqrt{3}R}\begin{pmatrix} 6 & -1 & -1 & -1 & -1 & -1 & -1 \\ -1 & 1 & 0 & 0 & 0 & 0 & 0 \\ -1 & 0 & 1 & 0 & 0 & 0 & 0 \\ -1 & 0 & 0 & 1 & 0 & 0 & 0 \\ -1 & 0 & 0 & 0 & 1 & 0 & 0 \\ -1 & 0 & 0 & 0 & 0 & 1 & 0 \\ -1 & 0 & 0 & 0 & 0 & 0 & 1 \end{pmatrix} \tag{51}$$

Thus, the second order tensor $\boldsymbol{M}$ introduced in (34) reads :

$$\boldsymbol{M} = m(T)\frac{16\sqrt{3}R}{X(\Delta\theta)}\frac{1}{49}\begin{pmatrix} 6 & -1 & -1 & -1 & -1 & -1 & -1 \\ -1 & 41 & -8 & -8 & -8 & -8 & -8 \\ -1 & -8 & 41 & -8 & -8 & -8 & -8 \\ -1 & -8 & -8 & 41 & -8 & -8 & -8 \\ -1 & -8 & -8 & -8 & 41 & -8 & -8 \\ -1 & -8 & -8 & -8 & -8 & 41 & -8 \\ -1 & -8 & -8 & -8 & -8 & -8 & 41 \end{pmatrix} \tag{52}$$

Hence the evolution law (33) for the hexagonal situation :

$$\dot{\boldsymbol{w}} = -m(T)\frac{8}{7}\frac{G(T)}{G(0)}\frac{\gamma(\Delta\theta)}{X(\Delta\theta)}\left(6,-1,-1,-1,-1,-1,-1\right)^T \tag{53}$$

Thus, by using (22) one obtains the inward normal speed according to the proposed model :

$$v = m(T)\frac{2}{R}\frac{G(T)}{G(0)}\frac{\gamma(\Delta\theta)}{X(\Delta\theta)} \tag{54}$$

The comparison between the inward normal speed from the curvature driven model (45) and from the proposed approach (54) reads :

$$m(T) = \widetilde{m}(T,\Delta\theta)\frac{X(\Delta\theta)}{2} \tag{55}$$

For sake of simplicity it is assumed that $\widetilde{m}(T,\Delta\theta)X(\Delta\theta)$ does not significantly depend on the disorientation :

$$\widetilde{m}(T,\Delta\theta)X(\Delta\theta) \approx \widetilde{\widetilde{m}}(T) \tag{56}$$

Hence :

$$m(T) \approx \frac{\widetilde{\widetilde{m}}(T)}{2} \tag{57}$$

where $\widetilde{\widetilde{m}}(T)$ is the grain boundary mobility without dependence on grain disorientation. The pure iron grain boundary mobility has been determined by [27] :

$$\widetilde{\widetilde{m}}(T) = \beta\frac{D_{\text{Fe}}(T)V_m\delta}{b^2\text{R}T} \tag{58}$$

where the molar volume of fcc-Fe is $V_m = 7.09.10^{-6}$ m^3, the boundary thickness is $\delta = 1$ nm, the burgers vector is $b = 2.48.10^{-10}$ m, the gas constant is R $= 8.3144621$ J.mol^{-1}.K^{-1}. In addition, $D_{\text{Fe}}(T)$ is the diffusivity of Fe atoms along the grain boundary (for fcc) and follows an Arrhenius law :

$$D_{\text{Fe}}(T) = D^0_{\text{Fe}}\exp\left(-\frac{Q}{\text{R}T}\right) \tag{59}$$

where the pre-factor is $D^0_{\text{Fe}} = 1.5.10^{-4}$ m^2.s^{-1} the activation energy is $Q = 148$ kJ.mol^{-1}.

7 Time discretization and numerical results

The temperature kinetics is imposed in the following, thus $T(t)$ is a known function. Voronoi-Laguerre tessellations $(\boldsymbol{x},\boldsymbol{y},\boldsymbol{w})$ are generated with the free software *Neper* [28] and orientations $\boldsymbol{\theta}$ are set in *Scilab* [26]. Weights are initially set to a common value and are updated at each time step according to the evolution law (33) and the driving force (42). The numerical discretization consists in a simple explicit scheme with adaptive time step in order to capture accurately growth rate variations. The time step is determined as follows :

$$N = \left\|\boldsymbol{M}(T,\boldsymbol{\alpha}).\frac{\partial\mathcal{E}(T,\boldsymbol{\alpha})}{\partial\boldsymbol{w}}\right\| \tag{60}$$

$$\text{d}t = \frac{\delta_w}{N} \tag{61}$$

where $\delta_w > 0$ is a constant value. As the simple model proposed in this paper is purely viscous, even though the temperature is maintained constant, grain growth never stops strictly speaking. The evolution

becomes only slower and slower. Thus, a stopping criterion needs to be defined. The algorithm is simply presented in figure 7.

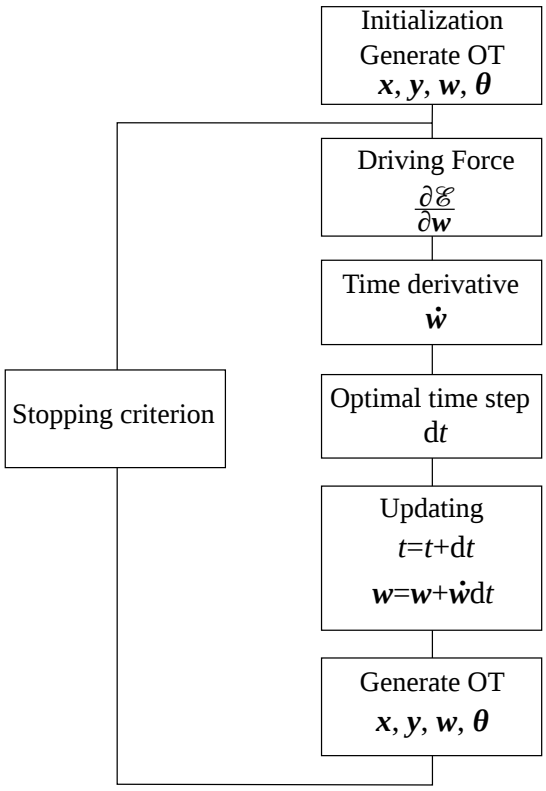

FIGURE 7 – Algorithm

Different *Orientated Tessellations* with different distributions of sphericity and grain size are generated. The orientation field correspond to a disorientation distribution very similar for each OT as shown in figure 8. The temperature is set to $T = 800$ K and grain growth is simulated by *Orientated Tessellation Updating Method* during approximatively 4 hours. The code is not optimized as *Scilab* has been used to compute the evolution law and *Neper* to generate tessellations. (Computation time is roughly 15 min for 1000 time steps and is mainly due to writting and reading text files between *Scilab* and *Neper*. Thus, a unifed code not relying on text files would significantly reduce computation time.)

Grain growth at 800 K is presented for three OT (denoted by OT1, OT2, OT3) in figures 9,11 and 12 (orientations are in degrees). Simulations show grain coarsing and are consistent with experimental observations [29] on an other material (tantalum). Grain growth is heterogeneous depending on the local disorientation and grain size arrangement leading to heterogenous grain size distribution during the transiant state. Of course, grain size heterogenities eventually reduce as bigger grain tends to grow at the expense of smaller grains. In addition, the disorientation distribution tends to favor small disorientations as shown in figure 8. Sphericity tends to increase as shown in figure 11 but this may be due to the fact that weights $\boldsymbol{w}$ are the only state variables. Future developments will include seeds $\boldsymbol{x}$ and $\boldsymbol{y}$ as state variables, which will enable to consider additional degrees of freedom to approximate more accurately grain shape evolution. In addition, orientations $\boldsymbol{\theta}$ can also be added as state variables with an associated dissipative mechanism related to crystal plasticity in the grain bulk. Thus, reorientation is likely to occur for small grain sizes as suggested by molecular dynamics [14] because reorientation involves dissipated energy per unit volume although grain boundary migration involves dissipated energy per unit area.

Grain growth is a thermally activated process as captured by the Arrhenius law (59). This is illustrated by simulating the same OT as those presented in figure 9 at 700 K. The resulting evolution is much slower than at 800 K as shown in figure 10.

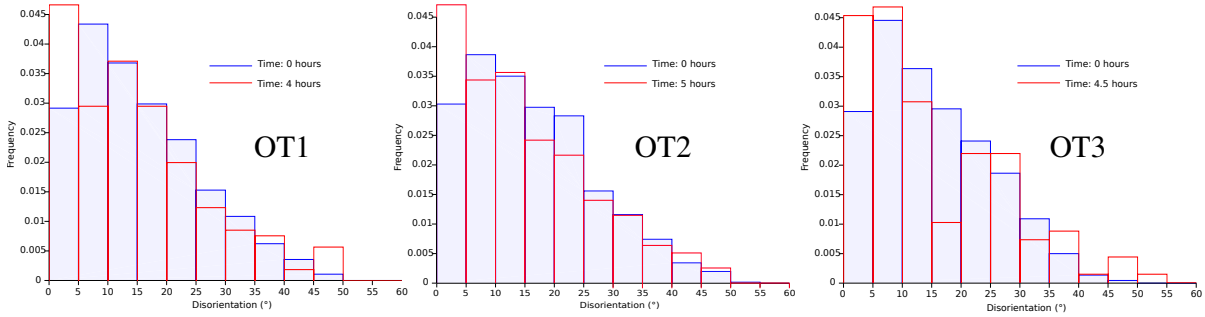

FIGURE 8 – Disorientation distributions of three OT at 800 K

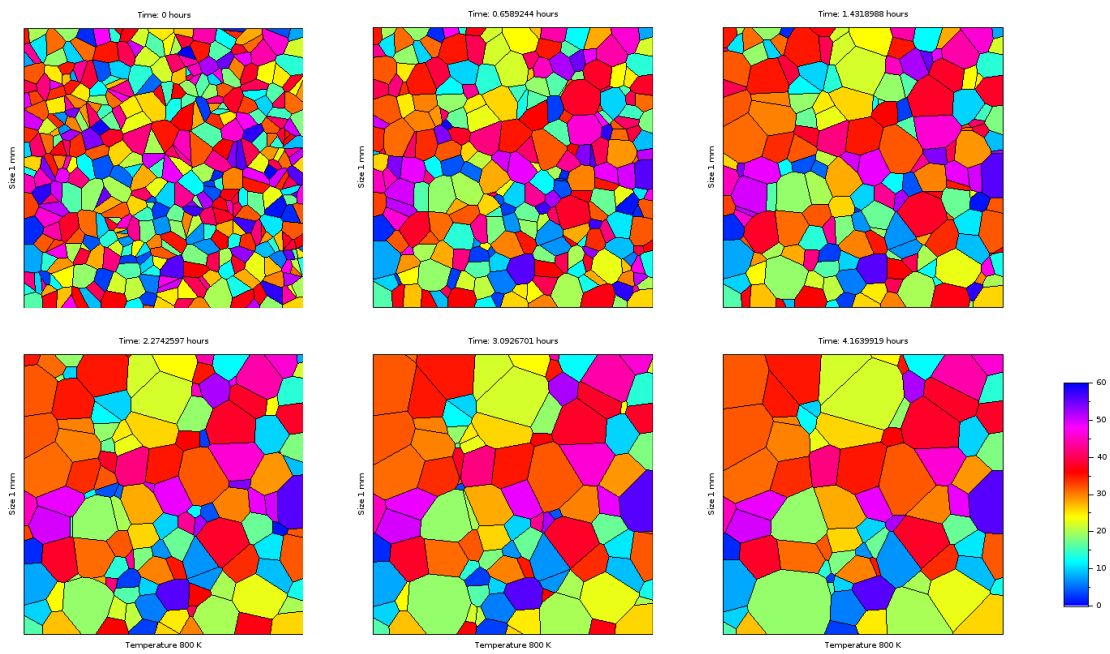

FIGURE 9 – Grain growth of the OT1 at 800 K during approximatively 4 hours

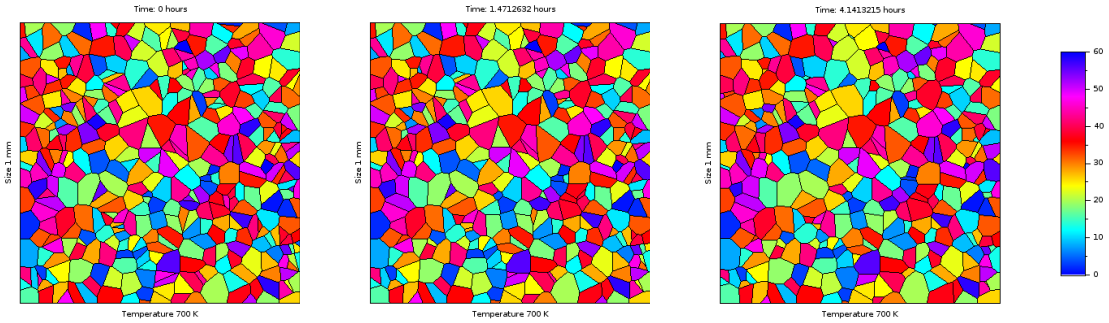

FIGURE 10 – Grain growth of the OT1 at 700 K during approximatively 4 hours

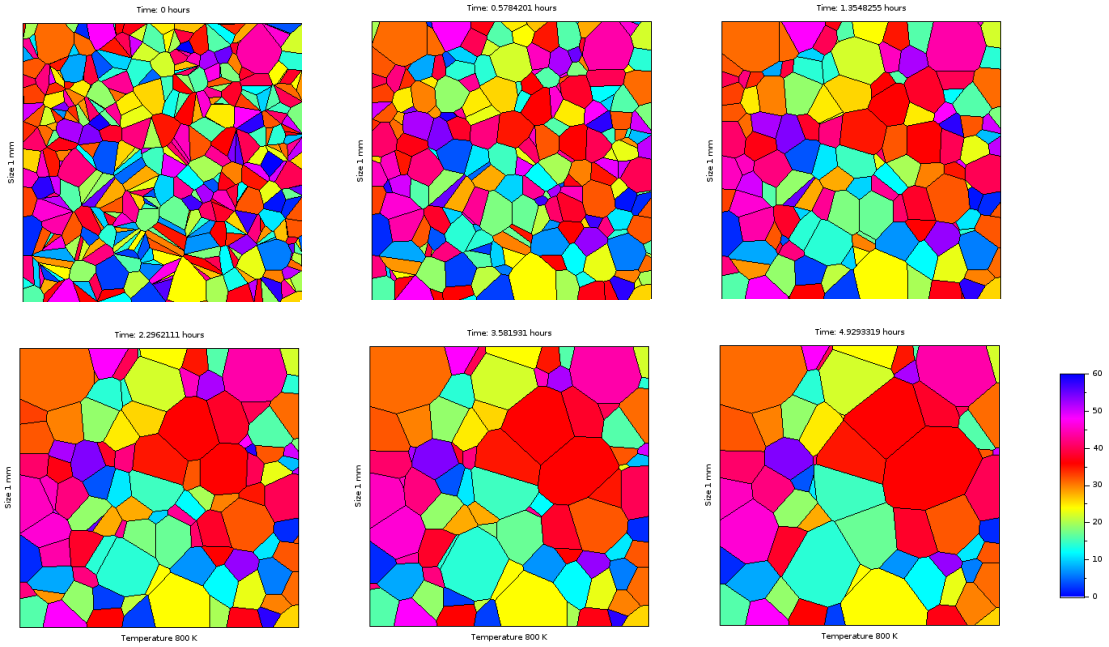

FIGURE 11 – Grain growth of the OT2 at 800 K during approximatively 4 hours

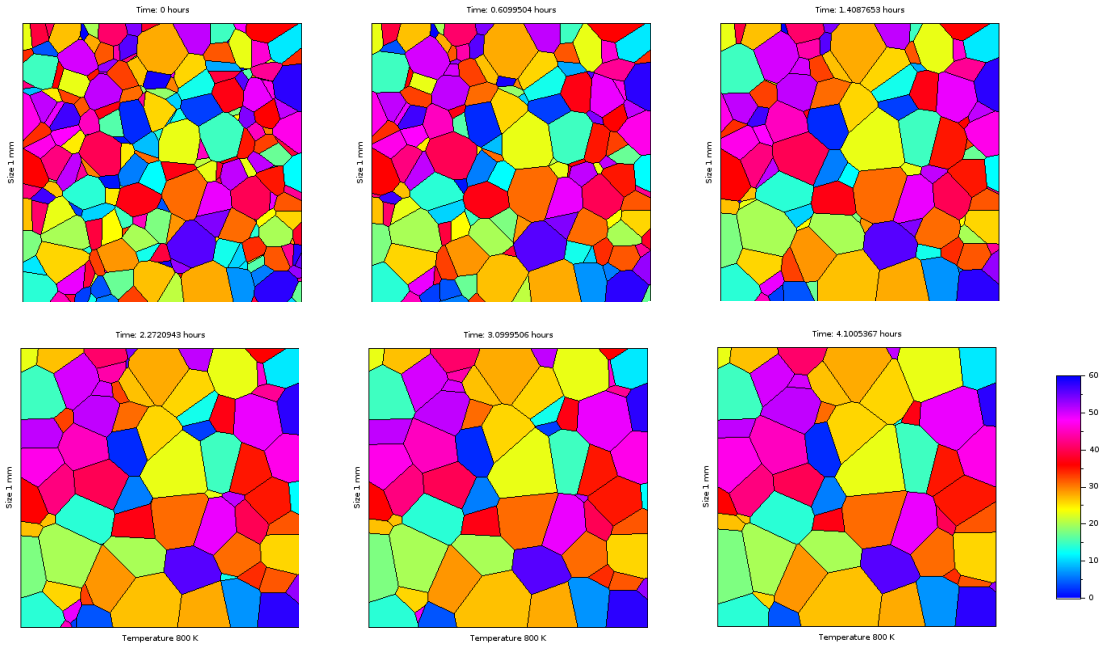

FIGURE 12 – Grain growth of the OT3 at 800 K during approximatively 4 hours

8 Conclusion

In this paper the *Orientated Tessellation Updating Method* has been introduced to simulate grain growth at *mesoscale* (i.e., at the scale of the polycrystalline structure) . The method relies on Voronoi-Laguerre tessellation techniques and energetic contributions at *microscale* (i.e., at the scale of the grain boundary), namely the grain boundary energy due to the crystal disorientation and the dissipated power by crystal plasticity for any virtual motion of the grain boundary. The method is very light in terms of computation cost. Even though 2D structures have been studied in this contribution, the extension in 3D is straightforward and future works will focus on this aspect. In addition, the only state variables are the weights of the tessellation. Thus, further developments including seeds and orientations as state variables are needed to approximate more accurately structural evolution of polycrystals. Furthermore, tessellation techniques include options to generate subgrain structures that could also be introduced in the framework presented in this paper.

Références

[1] Daniel Kandel and Eytan Domany. Rigorous derivation of domain growth kinetics without conservation laws. *Journal of Statistical Physics*, 58(3-4) :685–706, 1990.

[2] Elizabeth A Holm, Gregory N Hassold, and Mark A Miodownik. On misorientation distribution evolution during anisotropic grain growth. *Acta Materialia*, 49(15) :2981–2991, 2001.

[3] Elizabeth A Holm, Mark A Miodownik, and Anthony D Rollett. On abnormal subgrain growth and the origin of recrystallization nuclei. *Acta Materialia*, 51(9) :2701–2716, 2003.

[4] Liangzhe Zhang, Anthony D Rollett, Timothy Bartel, Di Wu, and Mark T Lusk. A calibrated monte carlo approach to quantify the impacts of misorientation and different driving forces on texture development. *Acta Materialia*, 60(3) :1201–1210, 2012.

[5] Jason Gruber, Denise C George, Andrew P Kuprat, Gregory S Rohrer, and Anthony D Rollett. Effect of anisotropic grain boundary properties on grain boundary plane distributions during grain growth. *Scripta materialia*, 53(3) :351–355, 2005.

[6] Håkan Hallberg. Influence of anisotropic grain boundary properties on the evolution of grain boundary character distribution during grain growth—a 2d level set study. *Modelling and Simulation in Materials Science and Engineering*, 22(8) :085005, 2014.

[7] Benjamin Scholtes, Romain Boulais-Sinou, Amico Settefrati, Daniel Pino Muñoz, Isabelle Poitrault, Aurore Montouchet, Nathalie Bozzolo, and Marc Bernacki. 3d level set modeling of static recrystallization considering stored energy fields. *Computational Materials Science*, 122 :57–71, 2016.

[8] N Ma, A Kazaryan, SA Dregia, and Y Wang. Computer simulation of texture evolution during grain growth : effect of boundary properties and initial microstructure. *Acta Materialia*, 52(13) :3869–3879, 2004.

[9] CE Krill Iii and L-Q Chen. Computer simulation of 3-d grain growth using a phase-field model. *Acta materialia*, 50(12) :3059–3075, 2002.

[10] Liesbeth Vanherpe, Nele Moelans, Bart Blanpain, and Stefan Vandewalle. Bounding box framework for efficient phase field simulation of grain growth in anisotropic systems. *Computational Materials Science*, 50(7) :2221–2231, 2011.

[11] Kunok Chang and Nele Moelans. Effect of grain boundary energy anisotropy on highly textured grain structures studied by phase-field simulations. *Acta Materialia*, 64 :443–454, 2014.

[12] M Upmanyu, DJ Srolovitz, LS Shvindlerman, and G Gottstein. Misorientation dependence of intrinsic grain boundary mobility : simulation and experiment. *Acta materialia*, 47(14) :3901–3914, 1999.

[13] M Upmanyu, DJ Srolovitz, LS Shvindlerman, and G Gottstein. Molecular dynamics simulation of triple junction migration. *Acta materialia*, 50(6) :1405–1420, 2002.

[14] M Upmanyu, David J Srolovitz, AE Lobkovsky, James A Warren, and WC Carter. Simultaneous grain boundary migration and grain rotation. *Acta Materialia*, 54(7) :1707–1719, 2006.

[15] FJ Humphreys. Modelling mechanisms and microstructures of recrystallisation. *Materials Science and Technology*, 8(2) :135–144, 1992.

[16] Fumihiro Wakai, Naoya Enomoto, and Hiroshi Ogawa. Three-dimensional microstructural evolution in ideal grain growth—general statistics. *Acta Materialia*, 48(6) :1297–1311, 2000.

[17] M Syha and D Weygand. A generalized vertex dynamics model for grain growth in three dimensions. *Modelling and Simulation in Materials Science and Engineering*, 18(1) :015010, 2009.

[18] Alexander Vondrous, Mathias Reichardt, and Britta Nestler. Growth rate distributions for regular two-dimensional grains with read–shockley grain boundary energy. *Modelling and Simulation in Materials Science and Engineering*, 22(2) :025014, 2014.

[19] William T Read and W Shockley. Dislocation models of crystal grain boundaries. *Physical review*, 78(3) :275, 1950.

[20] Dieter Wolf. A read-shockley model for high-angle grain boundaries. *Scripta Metallurgica*, 23(10) :1713–1718, 1989.

[21] Vasily V Bulatov, Bryan W Reed, and Mukul Kumar. Grain boundary energy function for fcc metals. *Acta Materialia*, 65 :161–175, 2014.

[22] A Kagawa, T Okamoto, and H Matsumoto. Young's modulus and thermal expansion of pure iron-cementite alloy castings. *Acta Metallurgica*, 35(4) :797–803, 1987.

[23] Tianbao Cheng, Daining Fang, and Yazheng Yang. The temperature dependence of grain boundary free energy of solids. *Journal of Applied Physics*, 123(8) :085902, 2018.

[24] Maurizio Brocato, Alain Ehrlacher, and Philippe Tamagny. Détermination de la dissipation caractéristique dans la propagation d'un front de recristallisation. *Comptes Rendus de l'Académie des Sciences-Series IIB-Mechanics-Physics-Astronomy*, 327(2-3) :179–184, 1999.

[25] Maurizio Brocato, Alain Ehrlacher, and Philippe Tamagny. Stability of discontinuities in polycrystals. *Waves and Stability in Continuous Media*, page 57, 1999.

[26] Scilab. Scilab : Free and open source software for numerical computation. *Scilab Enterprises, Orsay, France*, 2012.

[27] CW Sinclair, CR Hutchinson, and Yves Brechet. The effect of nb on the recrystallization and grain growth of ultra-high-purity α-fe : a combinatorial approach. *Metallurgical and Materials Transactions A*, 38(4) :821–830, 2007.

[28] Romain Quey, PR Dawson, and Fabrice Barbe. Large-scale 3d random polycrystals for the finite element method : Generation, meshing and remeshing. *Computer Methods in Applied Mechanics and Engineering*, 200(17-20) :1729–1745, 2011.

[29] Christophe Kerisit, Roland E Logé, Suzanne Jacomet, Valérie Llorca, and Nathalie Bozzolo. Ebsd coupled to sem in situ annealing for assessing recrystallization and grain growth mechanisms in pure tantalum. *Journal of microscopy*, 250(3) :189–199, 2013.